Bioorganic & Medicinal Chemistry Letters 22 (2012) 4979–4985

Contents lists available at SciVerse ScienceDirect

Bioorganic & Medicinal Chemistry Letters

journal homepage: www.elsevier.com/locate/bmcl

The design, synthesis, and biological evaluation of potent receptor tyrosine kinase inhibitors

Moon H. Kim, Amy Lew Tsuhako *, Erick W. Co, Dana T. Aftab, Frauke Bentzien, Jason Chen, Wei Cheng, Stefan Engst, Levina Goon, Rhett R. Klein, Donna T. Le, Morrison Mac, Jason J. Parks, Fawn Qian, Monica Rodriquez, Thomas J. Stout, Jeffrey H. Till, Kwang-Ai Won, Xiang Wu, F. Michael Yakes, Peiwen Yu, Wentao Zhang, Yeping Zhao, Peter Lamb, John M. Nuss, Wei Xu

Exelixis, 210 E. Grand Avenue, South San Francisco, CA 94080, USA

ARTICLE INFO

Article history:
Received 4 May 2012
Revised 6 June 2012
Accepted 11 June 2012
Available online 16 June 2012

Keywords:
Receptor tyrosine kinase
Angiogenesis
KDR
VEGFR
Flt
FGFR
PDGFR
Oxindole
Indolin-2-one

ABSTRACT

Variously substituted indolin-2-ones were synthesized and evaluated for activity against KDR, Flt-1, FGFR-1 and PDGFR. Extension at the 5-position of the oxindole ring with ethyl piperidine (compound **7i**) proved to be the most beneficial for attaining both biochemical and cellular potencies. Further optimization of **7i** to balance biochemical and cellular potencies with favorable ADME/ PK properties led to the identification of **8h**, a compound with a clean CYP profile, acceptable pharmacokinetic and toxicity profiles, and robust efficacy in multiple xenograft tumor models.

Vascular endothelial growth factor receptor 1 (VEGFR1 or fms-like tyrosine kinase receptor, Flt-1) and vascular endothelial growth factor receptor 2 (VEGFR2 or kinase insert domain receptor, KDR) are receptor tyrosine kinases (RTKs) that regulate endothelial cell function.[1] Upon binding to members of the VEGF family of growth factors, these receptors undergo dimerization and autophosphorylation, and initiate a cascade of intracellular downstream signaling that promotes angiogenesis. Induction of angiogenesis is thought to be required for the ongoing growth of human tumors and consequently, targeting angiogenesis via inhibition of the VEGF pathway has been a prevalent approach to cancer therapy.[2,3]

Selective inhibition of VEGF signaling, best exemplified by the use of bevacizumab, has shown limited efficacy as a single therapeutic approach, but has been highly successful when used in combination with chemotherapy.[4–6] One possible explanation for the limited single agent activity is the presence of alternate mechanisms for the promotion of angiogenesis.[7,8] Studies in pre-clinical tumor models suggest that both platelet-derived growth factor

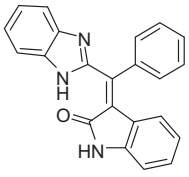

1

KDR: 97 nM; **FGFR1**: 95 nM
PDGFRα: 261 nM

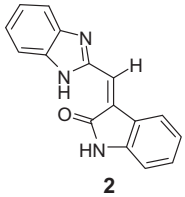

2

KDR: >4880 nM; **FGFR1**: >4880 nM
Flt-1: 405 nM

Figure 1. Lead Compound **1** and the corresponding des-phenyl analog.

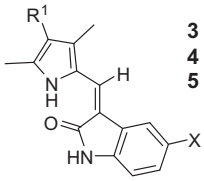

3 Sunitinib: R^1=CONH(CH_2)N$(C_2H_5)_2$; X = F
4 SU5416: R^1 = H; X = H
5 SU6668: R^1 = $(CH_2)_2$COOH; X = H

Figure 2. Oxindole VEGFR-2 inhibitors.

* Corresponding author. Tel.: +1 650837 8042.
E-mail addresses: amy.lew@gmail.com, alew@exelixis.com (A.L. Tsuhako).

0960-894X/$ - see front matter © 2012 Elsevier Ltd. All rights reserved.
http://dx.doi.org/10.1016/j.bmcl.2012.06.029

Table 1
Biochemical inhibitory activity for A, B, C ring oxindole modifications

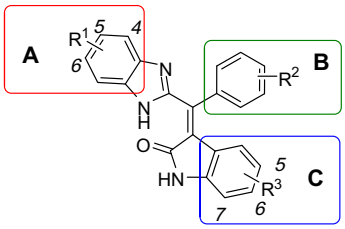

ID	R^1	R^2	R^3	Kinase inhibitory activity IC_{50}[a] (nM)		
				KDR	Flt-1	FGFR1
3	–			37	1	1064
5	–			135	28	1950
6a	H	*o*-Me	H	97	618	205
6b	H	*m*-Me	H	119	681	814
6c	H	*p*-Me	H	88	599	187
6d	H	*p*-F	H	633	2308	950
6e	H	*m*-F	H	125	522	79
6f	H	3,5-Di-F	H	106	2551	4000
6g	H	2,4-Di-F	H	290	1796	628
6h	H	*p*-CF_3	H	19903	24000	4899
6i	H	2,4-Di-Cl	H	2180	24400	725
6j	H	*p*-OMe	H	327	984	86
6k	H	*p*-OEt	H	9876	10543	6293
6l	H	*p*-NH_2	H	68	371	57
6m	H	H	5-Br	51	118	446
6n	H	H	6-Br	4880	4544	4880
6o	H	H	7-Br	4880	4880	4880
6p	H	H	5-COOH	4	39	75
6q	H	H	6-COOH	213	582	1586
6r	H	H	7-COOH	23633	20716	24400
6s	H	H	5-NH_2	32	201	13
6t	H	*p*-Me	5-COOH	5	45	67
6u	H	*p*-Me	5-NH_2	82	473	51
6v	5-OMe	H	5-COOH	3	77	39
6w	5-OMe	H	5-NH_2	60	377	42

[a] Values reported are the average of at least two independent dose-response curves; variation was generally ±15%.[35]

receptor (PDGFR) and fibroblast growth factor receptor (FGFR) activation can contribute to angiogenesis and promote resistance to VEGF-pathway targeting agents.[9,10]

Multiple first generation small molecule inhibitors of the VEGFR pathway are currently on the market or in clinical trials.[2,3] A number of these combine inhibition of VEGFRs with other RTKs, including PDGFRs, FGFRs or EGFRs. AG-013736 (Axitinib)[11,12] CHIR-258/TKI258 (Dovitinib),[13] BIBF 1120 (Vargatef),[14] AZD2171 (Cediranib),[15] and BMS-540215 (Brivanib)[16] are examples of small molecule inhibitors that target VEGFRs in combination with other RTKs. Emerging clinical evidence suggests that these single agents may have a broader spectrum of activity than highly selective VEGF targeting agents.[17] Given the limited activity of selective VEGF-pathway inhibitors, we sought to optimize a second generation angiogenesis inhibitor that would target multiple pro-angiogenic pathways simultaneously through balanced inhibition of VEGFRs, PDGFRs and FGFRs.

Our efforts began with high throughput screening (HTS) of our internal small molecules library against KDR, leading to the identification of oxindole **1** with modest activities against KDR, FGFR1, and PDGFRα (Fig. 1). Several oxindoles[14,18–23] or oxindole-like compounds[24–26] have been documented in the literature as RTK inhibitors, with sunitinib,[27] currently approved to treat kidney, pancreatic, and gastrointestinal cancers (Fig. 2). However, as opposed to HTS hit **1**, sunitinib (**3**) does not have a phenyl group on the substituted alkene (Comparison of Fig. 2, compound **3** with Fig. 1, compound **1**). Removal of this phenyl ring on HTS hit **1**, rendered the analog inactive against VEGFR and FGFR1 (Compound **2**, Fig. 1). Similar to compound **2**, sunitinib (**3**), in the absence of the phenyl substitution, was also inactive against FGFR1 (Table 1). With such dramatic differences in KDR and FGFR activities in the presence/absence of the phenyl ring substitution on the alkene, we felt that there was unexplored SAR in this region. Herein, we describe optimization efforts of **1** that led to the discovery of compound **8h**.

Efforts towards establishing SAR around **1** were focused on varying substituents in the B and C rings, two areas less explored in oxindoles targeted against KDR. In the phenyl B ring, a variety of *ortho*, *meta*, and *para* substituents were explored (Table 1). Small substituents were tolerated in this region, as *ortho*-, *meta*-, and *para*- methyl and fluoro substitutions retained KDR activity (**6a**–**6e**). However, once the substituents were larger, such as the dichloro (**6i**), or *p*-ethoxy (**6k**) groups, KDR activity was dramatically decreased. In addition, the *para*-position was less tolerant of electron withdrawing functional groups as the *p*-F (**6d**) was less potent than the *m*-F (**6e**) analog and replacement of the active *p*-Me with *p*-CF_3 (**6h**) rendered the analog inactive. However, none of these B ring modifications were significantly more potent than HTS lead **1**.

As opposed to B ring modifications, a clear trend emerged from modifications in the C ring (Table 1). Placing substituents in the 5-position of the oxindole ring improved KDR potency. For example, in the bromide series (**6m**–**6o**), a 5-bromo substitution was 100-fold more active than a 6- or 7-bromo substitution. Likewise, a 5-carboxylate substitution was 50 to 1000-fold more potent than the corresponding 6- or 7- carboxylate substitution (**6p**–**6r**). Interestingly, both anilines and carboxylic acids were tolerated in

Table 2
Biochemical and cellular inhibitory activity for 5-amide, sulfonamide and amine oxindoles

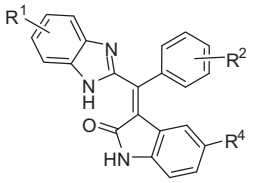

ID	R^1	R^2	R^4	Kinase inhibitory activity IC_{50}[a] (nM)				Cell based IC_{50}[a] (nM)	
				KDR	Flt-1	FGFR1	PDGFRα	KDR/ERK[b]	FGFR1/ERK[c]
7a	H	H	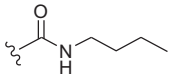	15	374	326	13	145	30000
7b	H	H	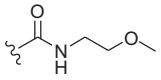	69	381	199	55	128	9666
7c	H	H	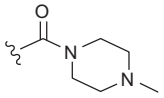	157	4322	70	–	1804	983
7d	H	H	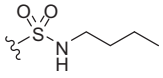	1134	24400	300	844	–	–
7e	H	H	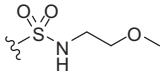	660	1950	287	614	30000	30000
7f	H	H	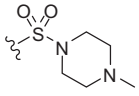	1950	1950	1950	1950	30000	30000
7g	5-OMe	H	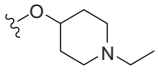	22	691	20	17	213	736
7h	5-OMe	H	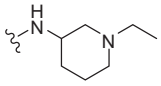	279	>1950	216	431	496	1010
7i	5-OMe	H	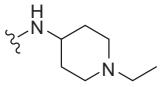	10	163	11	6	27	41
7j	H	H	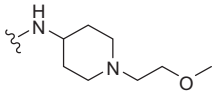	9	184	46	10	17	50

[a] Values reported are the average of at least two independent dose-response curves; variation was generally ±15%.[35,38,39]
[b] VEGF-stimulated ERK phosphorylation in human endothelial cells (HUVEC).
[c] FGF-stimulated ERK phosphorylation in SK-N-MC neuroblastoma cells.

the 5-position; although carboxylic acid derivatives were more potent than aniline derivatives (**6p** vs **6s**, **6t** vs **6u**, **6v** vs **6w**).

With encouraging data from the 5-amino and 5-carboxylate analogs, we focused on expanding the 5-position substitutions of the oxindole ring. Table 2 summarizes the amides, sulfonamides, and amines explored in the 5-position. In general, bulky amides were not tolerated, and primary amides were better than secondary amides. In addition, amide analogs were more potent in KDR, FGFR1 and PDGFRα than the corresponding sulfonamide analogs (**7a** vs **7d**, **7b** vs **7e**, **7c** vs **7f**). However, despite the fact that amide **7a** showed good biochemical potency, it was only modestly potent at inhibiting endogenously expressed VEGF and FGF receptor activity in human endothelial cells and human umbilical vein endothelial cell (HUVEC), respectively (Table 2). In contrast, the 5-amino piperidinyl oxindole series was very potent in cells (**7i**, **7j**). Regiochemistry of the amine was important as the 3-amino piperidine analog **7h** was significantly less potent than the 4-amino piperidine analog **7i**. Switching the 5-amino oxindole linkage to that of an ether linkage such as analog **7g**, still maintained KDR potency, but in general was less potent, especially against Flt-1.

To better understand the SAR observed for the 5-aminopiperidinyl series, **7i** was co-crystallized in EphB4 (IC_{50} = 765 nM), a surrogate receptor tyrosine kinase, since access to the crystal structure of KDR, FGFR or PDGFR was not available at the time of this study. The crystal structure showed that in addition to the triad of hydrogen bonds between the indolin-2-one core of **7i** and the hinge region, there was an additional hydrogen bond between the piperidine nitrogen and Asp234, the catalytic acid responsible for chelating magnesium in the reaction complex (Fig. 3). This interaction is also predicted to be present in KDR and could account for the increase in potency observed for **7g**, **7i**, and **7j**. To the best of our knowledge, the interaction of this aminopiperidinyl functional group with the kinase had not previously been described for oxindole-based inhibitors of KDR. In addition, the phenyl B ring is tightly packed, forming primarily hydrophobic interactions with the protein. This tight packing likely contributes to the high

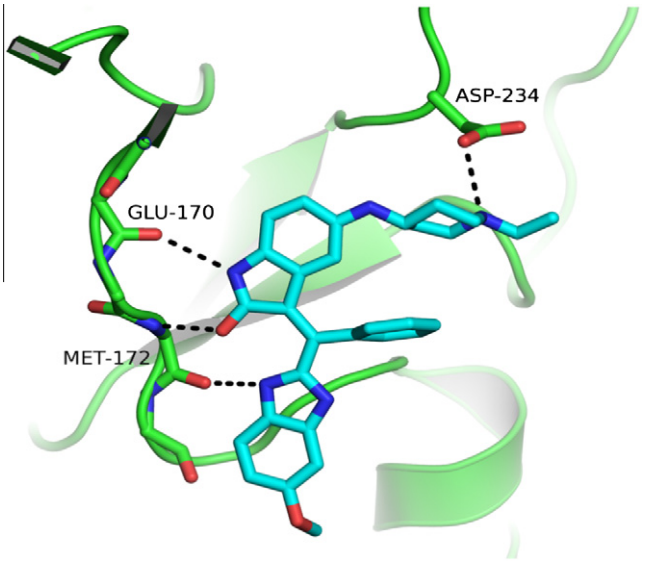

Figure 3. Crystal structure of EphB4, a surrogate receptor tyrosine kinase, co-crystallized with compound **7i** (PDB code 4AW5). Unique to the oxindole class targeting VEGFR, the 5-amino-piperidinyl moiety of **7i** is able to form a hydrogen bond with the catalytic ASP-234.

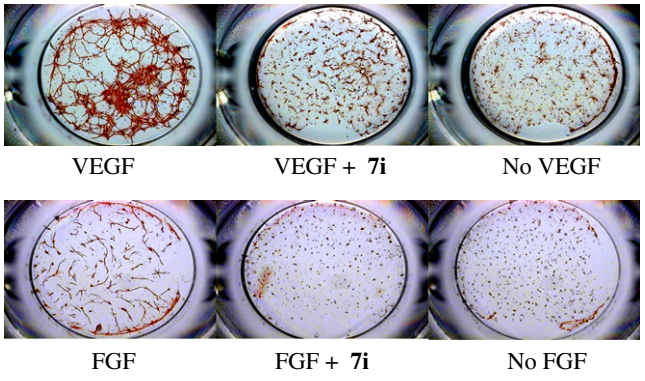

Figure 4. Effect of **7i** on capillary-like tube formation induced by VEGF and FGF.

	Vehicle		Compound **8h**, mg/kg					
	V-	V+	1	3	10	30	60	100
KDR								
pKDR								
Compared to V+	39	100	90	95	86	80	48	39
pKDR inh. %	-	-	10	5	14	20	52	61
plasma conc. μM	-	-	0.004	0.01	0.02	0.01	0.01	0.62
Lung conc. μM		-	<LOQ	0.07	0.28	0.47	0.81	3.55

Figure 5a. Pharmacodynamic studies for **8h** measuring inhibition of phosphorylated KDR in mouse lung tissue. V− is the basal level of KDR and pKDR while V+ is the level of KDR and pKDR before compound treatment, but after VEGF stimulation.[28] Lung tissue was analyzed 4 h post dose.

potency observed against KDR in this series and also explains the intolerance to larger substituents on the phenyl ring.

To ascertain whether the in vitro profile of **7i** correlated with anti-angiogenic properties, endothelial tube formation assays were performed. When plated on a confluent layer of normal human diploid fibroblast cells, human microvascular endothelial cell (HMVECS) form extensive networks of tubules in response to VEGF over a period of 7–10 days. Tubules are stained and quantitated

	Vehicle sunitinib		Compound **8h**, mg/kg					
	V	100	1	3	10	30	60	100
FGFR1								
pFGFR1								
Normalized to V	100	104	92	92	57	52	34	32
pFGFR1 inh. %	-	0	8	8	43	48	66	68
plasma conc. μM	-		<LOQ	0.01	0.04	0.20	0.26	0.80
Tumor conc. μM	-		<LOQ	<LOQ	0.34	1.40	3.60	8.80

Figure 5b. Pharmacodynamic studies for **8h** in MDA-MB231T xenograft model measuring inhibition of phosphorylation of FGFR1.

using an antibody that recognizes the endothelial cell marker CD31. Compound **7i** inhibits VEGF-induced tubule formation (Fig. 4) with an IC_{50} of 110 nM. Likewise, FGF-induced tubule formation was also tested in this system; and compound **7i** potently inhibits FGF-induced tubule formation with an IC_{50} of 10 nM (Fig. 4). Collectively, these data demonstrate that inhibition of VEGFR and FGFR by **7i** translates into potent inhibition of endothelial tube formation function in response to the key angiogenic factors VEGF and FGF.

With biochemical and cellular potencies optimized for the C-ring, and clear demonstration of anti-angiogenic properties in cells, we were now ready to re-optimize the A and B rings with the goal of improving ADME/PK properties. The 5-aminopiperidinyl oxindole analog **7i** showed CYP3A4 liabilities (CYP3A4 IC_{50}: 5.6 μM), high clearance (6497 mL/h/kg) and low oral availability (F = 19%) in rats. Holding the C ring constant as the 5-aminopiperidinyl oxindole, a variety of substituted and unsubstituted benzimidazoles and imidazoles were synthesized as the A ring in combination with a variety of substituted B rings. Highlights of these analogs are shown in Table 3.

With the 5-aminopiperidinyl substitution installed on the C ring, a majority of the analogs showed single digit nM potencies against KDR, FGFR, and PDGFR, and were below 100 nM in VEGF and FGF-driven cellular signaling assays (Table 3). As predicted, the benzimidazole A ring contributed significantly to the CYP3A4 activity. Surprisingly, when replaced with an imidazole or methyl imidazole, the CYP3A4 activity was attenuated (Table 3). For example, when the A ring benzimidazole of analog **8a** was replaced with an imidazole (**8f**), the CYP3A4 activity was abolished. Likewise, when the A ring benzimidazole of analog **8d** was replaced with an imidazole (**8g**) or methyl imidazole (**8i**), the CYP3A4 activity improved. In addition, we discovered that halogens on the B ring, especially a Cl or di-F, aided in improving oral bioavailability in rat pharmacokinetic studies (Table 3). Four compounds emerged (**8g**, **8h**, **8i**, and **8k**) with high potency against KDR, Flt-1, FGFR1 and PDGFRα, good cell activity, a clean CYP profile (>10 μM) and reasonable PK profile.

Of the four compounds, **8h** was chosen for in vivo pharmacodynamic studies due to its more favorable oral bioavailability (F = 63% in rats; Table 3). As shown in Figure 5a, single oral dose administration of **8h** resulted in a dose dependent decrease in VEGF-stimulated phosphorylation of KDR in lung lysates 4 h post dose. The plasma concentration dose response relationship predicts 50% inhibition of phosphorylation of KDR in vivo to occur at ~0.28 μM. The corresponding lung lysate concentration-response relationship indicates that 50% inhibition of phosphorylation of KDR is predicted to occur at a lung concentration of 1.6 μM. Note that the 100-mg/kg dose caused a reduction in phosphorylation of the receptor to levels below the basal phosphorylation state.

Table 3
Biochemical, cellular, and cytochrome P450 inhibitory activity for 5-amino ethyl piperidine oxindole analogs

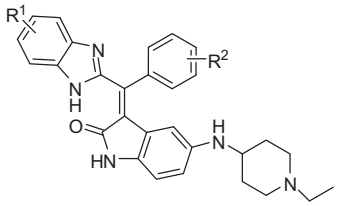

(**8a-8e**)

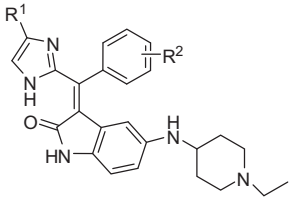

(**8f-8k**)

ID	R^1	R^2	Kinase inhibitory activity IC_{50}[a] (nM)				Cell based IC_{50}[a] (nM)		Rat PK dosed at 10 mg/kg (PO)			
			KDR	Flt-1	FGFR1	PDGFRα	KDR/ERK[b]	FGFR1/ERK[c]	CYP3A4 IC_{50} (μM)	$AUC_{(0-\infty)}$ (μM•h)	$t_{1/2}$ (h)	%F
8a	H	H	6	161	5	3	<10	17	3	1.44	5.7	37
8b	H	*p*-Me	8	112	10	5	<10	59	12	2.36	4.6	55
8c	H	*p*-OMe	13	96	14	7	13	44	9	0.33	7.5	27
8d	H	*m*-F	3	62	5	7	<10	38	4	1.99	4.4	63
8e	H	3,5-DiF	4	66	8	6	<10	46	6	3.14	3.8	72
8f	H	H	16	166	12	20	235	154	25	1.50	11.6	16
8g	H	*m*-F	7	25	13	6	20	17	23	1.12	5.4	15
8h	H	*p*-Cl	4	7	6	3	11	24	>50	5.04	10.7	63
8i	Me	*m*-F	4	20	4	2	6	20	25	1.90	4.6	20
8j	Me	3,5-DiF	3	11	7	3	7	24	10	5.19	7.2	59
8k	Me	*o*-F	3	29	8	5	16	15	26	1.03	2.3	25

[a] Values reported are the average of at least two independent dose-response curves; variation was generally ± 15%.[35,38,39]
[b] VEGF-stimulated ERK phosphorylation in human endothelial cells (HUVEC).
[c] FGF-stimulated ERK phosphorylation in SK-N-MC neuroblastoma cells.

In a separate experiment, **8h** was administered to mice bearing MDA-MB-231 xenograft tumors transfected with a stable construct expressing FGFR1. Dose dependent inhibition of phospho-FGFR1 was observed with the corresponding dose response relationship predicting 50% inhibition of phosphorylation of FGFR1 to occur at a plasma concentration of ~0.14 μM. Note that despite achieving significantly higher plasma concentrations when compared to **8h**, a 100-mg/kg dose of sunitinib did not result in inhibition of phosphorylation of FGFR1 (Fig. 5b).

The encouraging pharmacodynamic data for **8h** supported additional in vivo characterization. Mice bearing MDA-MBA-231 (breast adenocarcinoma) and HT29 (colon adenocarcinoma) xenograft tumors were orally administered **8h** once daily for 14 days, starting when tumors were approximately 100 mg in size. Dose dependent tumor growth inhibition was observed in both models, (Fig. 6), and was associated with significant reductions in tumor mean vessel density, consistent with an anti-angiogenic mechanism of action (data not shown). The estimated ED_{50} values were 35 and 28 mg/kg for MDA-MB-231 and HT29 models, respectively. The compound was well tolerated as no loss of body weight occurred during the dosing period. Antitumor efficacy in both models was associated with cyclical plasma exposure with peak concentrations of 1–5 μM.

The analogs in Tables 1–3 were prepared by heating benzimidazole **9b** together with benzoyl chloride **10** at 135 °C in the presence of triethyl amine and acetonitrile (Scheme 1).[29–31] Although, both N- and C- acylation of the benzimidazole occurred, refluxing the diacylated intermediate with 7% aqueous HCl for 30 min led to hydrolysis at the N-acylated site, and yielded the desired C-acylated benzimidazole ketone **11b**. The corresponding imidazole ketone **11a** was also synthesized in a similar manner. Subsequent aldol condensation of **11a** or **11b** with oxindole **12** in a sealed tube of ammonia in ethanol afforded the desired analogs, with high stereoselectivity.[32] X-ray analysis (data not shown) and 2D NMR (data not shown) also confirmed the *E*/*Z* stereoselectivity shown in Scheme 1. Non-commercially available oxindoles such as 5-sulfonamide oxindoles were synthesized via regioselective sulfonylation with chlorosulfonic acid, followed by amine addition to the corresponding 2-oxo-2,3-dihydro-1*H*-indole-5-sulfonyl chloride (Scheme 2).[33] The 5-aminopiperidinyl oxindole was synthesized

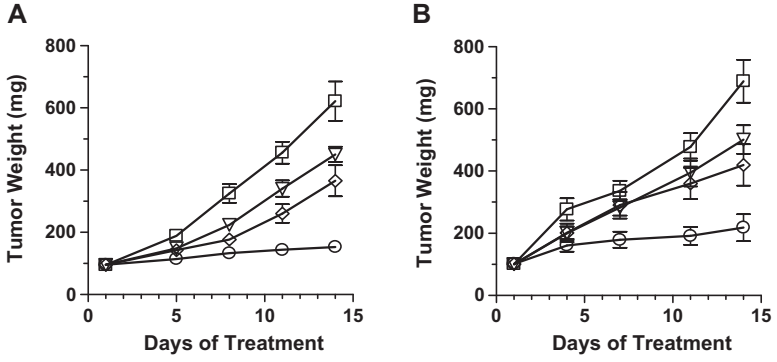

Figure 6. Xenograft efficacy for **8h**.[40] Female athymic mice bearing established MDA-MB-231 (A) and HT29 (B) xenograft tumors were orally administered **8h** at 10 mg/kg (), 30 mg/kg (◇), and 100 mg/kg (○) or saline vehicle (□) for 14 days. Tumor weights were determined twice weekly. Data points represent the mean tumor weight (in milligrams) and standard error for each treatment group.

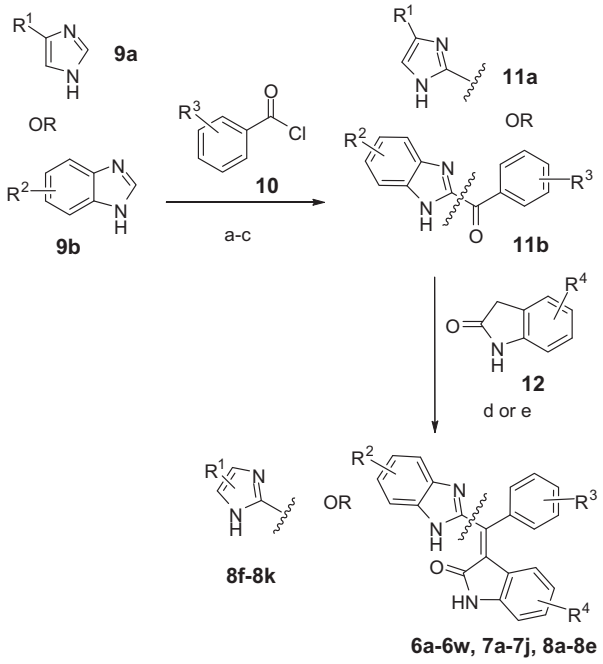

Scheme 1. Reagents and conditions: (a) Et_3N, CH_3CN, 135 °C, 2 h (b) 7% HCl, acetone, charcoal, reflux 30 min (c) NH_4OH (d) NH_3, EtOH, 90 °C (e) *N*,*N*-dimethylethylene diamine, EtOH, 90 °C.

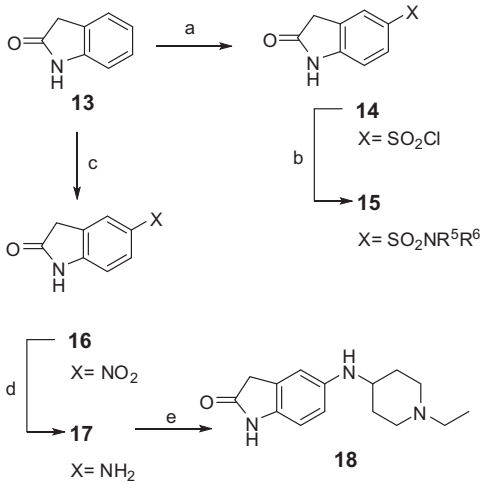

Scheme 2. Reagents and conditions: (a) $ClSO_3H$ (b) NHR^5R^6, DIEA, THF (c) KNO_3, H_2SO_4 (d) Pd/C, EtOH, H_2, 10–20 psi (e) 4-ethyl piperidone, $NaBH(OAc)_3$, HOAc, 1,2-DCE, 4 Å mol sieves.

via a regioselective nitration[34] of oxindole using potassium nitrate and sulfuric acid to give 5-nitro oxindole (**16**, Scheme 2), followed by reduction of the nitro group with palladium on carbon in ethanol to give the desired 5-amino oxindole **17**. Reductive amination of **17** with 4-ethyl piperidone and sodium triacetoxyborohydride then gave the desired 5-piperidinyl amino oxindole **18**. Analogs using the piperidinyl oxindole **18** or sulfonamide **15** were then made via an ammonia ethanol aldol condensation with the appropriate benzimidazole or imidazole ketones as previously described.

In summary, we obtained a potent, small molecule inhibitor of multiple angiogenic RTKs, starting from a lead oxindole identified by screening an in-house library for inhibitors of KDR Systematic modification around the core led to the identification of a 5-amino-piperidinyl functionality that significantly improved biochemical activity. Further optimization for favorable ADME/PK properties led to the development of **8h**,[41] a compound with an acceptable MDCK value (68 nM/sec), a *c*log*P* of 3.3, and a polar surface area of 73 Å.

This compound demonstrated potent activities against KDR, Flt-1, PDGFR, and FGFR1, which translated into robust pharmacodynamic and antitumor activity in vivo. When screened against a wider panel of kinases, **8h** also exhibited low nM inhibitory activity against several Src family tyrosine kinases (Src, and Yes), and several cell cycle and mitogen activated protein kinases (MAP4K3, and the Rsk family members), but was inactive against EGFR, EphB4/A2, IGFR, or IRK kinases. (Table 4). Although, preliminary hERG binding studies showed modest affinity for the ion channel (IC_{50} 3367 nM), we felt that **8h**'s high potency, warranted further investigation. On the basis of its favorable in vitro profile and in vivo efficacy, **8h** was advanced into further preclinical in vivo safety studies.

Table 4
Selectivity profile for **8h**

Kinase	Inhibitory activity for **8h** IC_{50}[a] (nM)
VEGFR family	
KDR (VEGFR-2)	4.2 ± 0.5
Flt-1 (VEGFR-1)	7.2 ± 0.8
Flt-4 (VEGFR-3)	3.2 ± 0.4
PDGFR family	
c-kit	11 ± 2
PDGFR-α	3.0 ± 0.3
PDGFR-β	1.3 ± 0.1
Flt-3	0.85 ± 0.19
Other tyrosine kinases	
FGFR1	5.7 ± 0.5
EGFR	137 ± 27
EphB4	1250 ± 60
EphA2	1700 ± 400
IGF-1R	2700 ± 400
IRK	4100 ± 200
Scr-family tyrosine kinases	
Src	33 ± 3
Yes[b]	—
Serine threonine kinases	
MAP4K3	25 ± 2
Rsk2	3.0

[a] Values reported are the average of at least two independent dose-response curves with the exceptions of values for Yes, MAP4K3, and Rsk where only one IC_{50} value was obtained.
[b] Compound **8h** inhibited Yes with 99% inhibition when tested at 1 μM.

Acknowledgments

We greatly appreciate the contributions to the biochemical, cellular, ADME/PK, and in vivo PD and efficacy data from members of the Exelixis Genome Biochemistry, New Lead Discovery, Cell Culture Facility, Pharmacology and Compound Repository.

References and notes

1. Ferrara, N.; Gerber, H. P.; LeCouter, J. *Nat. Med.* **2003**, *9*, 669.
2. Paz, K.; Zhu, Z. *Front. Biosci.* **2005**, *10*, 1415.
3. Ivy, S. P.; Wick, J. Y.; Kaufman, B. M. *Nat. Rev. Clin. Oncol.* **2009**, *6*, 569.
4. Hurwitz, H.; Fehrenbacher, L.; Novotny, W.; Cartwright, T.; Hainsworth, J.; Heim, W.; Berlin, J.; Baron, A.; Griffing, S.; Holmgren, E.; Ferrara, N.; Fyfe, G.; Rogers, B.; Ross, R.; Kabbinavar, F. *N. Eng. J. Med.* **2004**, *350*, 2335.
5. Ferrara, N.; Hillan, K. J.; Novotny, W. *Biochem. Biophys. Res. Commun.* **2005**, *333*, 328.
6. Cohen, M. H.; Gootenberg, J.; Keegan, P.; Pazdur, R. *Oncologist* **2007**, *12*, 713.
7. Bergers, G.; Hanahan, D. *Nat. Rev. Cancer* **2008**, *8*, 592.
8. Gordon, M. S. *Expert Rev. Anticancer Ther.* **2011**, *11*, 485.
9. Thurnher, A.; Katsen, A. D.; Groth, G.; Kerger, H.; Hammes, H-P.; Menger, M. D.; Ullrich, A.; Vajkoczy, P. *FASEB J.* **2004**, *18*, 338.
10. Casanovas, O.; Hicklin, D. J.; Bergers, G.; Hanahan, D. *Cancer Cell* **2005**, *8*, 299.

11. Hu-Lowe, D. D.; Zou, H. Y.; Grazzini, M. L.; Hallin, M. E.; Wickman, G. R.; Amundson, K.; Chen, J. H.; Rewolinski, D. A.; Yamazaki, S.; Wu, E. Y.; McTigue, M. A.; Murray, B. W.; Kania, R. S.; O'Connor, P.; Shalinsky, D. R.; Bender, S. L. *Clin. Cancer Res.* **2008**, *14*, 7272.
12. Rugo, H. S.; Herbst, R. S.; Liu, G.; Park, J. W.; Kies, M. S.; Steinfeldt, H. M.; Pithavala, Y. K.; Reich, S. D.; Freddo, J. L.; Wilding, G. *J. Clin. Oncol.* **2005**, *23*, 5474.
13. Sarker, D. *Clin. Cancer Res.* **2008**, *14*, 2075.
14. Hilberg, F.; Roth, G. J.; Krssak, M.; Kautschitsch, S.; Sommergruber, W.; Tontsch-Grunt, U.; Garin-Chesa, P.; Bader, G.; Zoephel, A.; Quant, J.; Heckel, A.; Rettig, W. J. *Cancer Res.* **2008**, *68*, 4774.
15. Wedge, S. R.; Kendrew, J.; Hennequin, L. F.; Valentine, P. J.; Barry, S. T.; Brave, S. R.; Smith, N. R.; James, N. H.; Dukes, M.; Curwen, J. O.; Chester, R.; Jackson, J. A.; Boffey, S. J.; Kilburn, L. L.; Barnett, S.; Richmond, G. H. P.; Wadsworth, P. F.; Walker, M.; Bigley, A. L.; Taylor, S. T.; Cooper, L.; Beck, S.; Jürgensmeier, J. M.; Ogilvie, D. J. *Cancer Res.* **2005**, *65*, 4389.
16. Huynh, H.; Ngo, V. C.; Fargnoli, J.; Ayers, M.; Soo, K. C.; Koong, H. N.; Thng, C. H.; Ong, H. S.; Chung, A.; Chow, P.; Pollock, P.; Byron, S.; Tran, E. *Clin. Cancer Res.* **2008**, *14*, 6146.
17. Arnold, D.; Seufferlein, T. *Gut* **2010**, *59*, 838.
18. Motzer, R. J.; Michaelson, M. D.; Redman, B. G.; Hudes, G. R.; Wilding, G.; Figlin, R. A.; Ginsberg, M. S.; Kim, S. T.; Baum, C. M.; DePrimo, S. E.; Li, J. Z.; Bello, C. L.; Theuer, C. P.; George, D. J.; Rini, B. I. *J. Clin. Oncol.* **2006**, *24*, 1.
19. Demetri, G. D.; Van Oosterom, A. T.; Garrett, C. R.; Blackstein, M. E.; Shah, M. H.; Verweij, J.; McArthur, G.; Judson, I. R.; Heinrich, M. C.; Morgan, J. A.; Desai, J.; Fletcher, C. D.; George, S.; Bello, C. L.; Huang, X.; Baum, C. M.; Casali, P. G. *Lancet* **2006**, *368*, 1329.
20. Sun, L.; Tran, N.; Liang, C.; Tang, F.; Rice, A.; Schreck, R.; Waltz, K.; Shawver, L. K.; McMahon, G.; Tang, C. *J. Med. Chem.* **1999**, *42*, 5120.
21. Laird, A. D.; Vajikoczy, P.; Shawver, L. K.; Thurnher, A.; Liang, C.; Mohammadi, M.; Schlessinger, J.; Ullrich, A.; Hubbard, S. R.; Blake, R. A.; Fong, T. A. T.; Strawn, L. M.; Sun, L.; Tang, C.; Hawtin, R.; Tang, F.; Shenoy, N.; Hirth, K. P.; McMahon, G.; Cherrington, J. M. *Cancer Res.* **2000**, *60*, 4152.
22. Sun, L.; Tran, N.; Liang, C.; Hubbard, S.; Tang, F.; Lipson, K.; Schreck, R.; Zhou, Y.; McMahon, G.; Tang, C. *J. Med. Chem.* **2000**, *43*, 2655.
23. Khanwelkar, R. R.; Chen, G. S.; Wang, H. C.; Yu, C. W.; Huang, C. H.; Lee, O.; Chen, C. H.; Hwang, C. S.; Ko, C. H.; Chou, N. T.; Lin, M. W.; Wang, L. M.; Chen, Y. C.; Hseu, H.; Chang, C. N.; Hsu, H. C.; Lin, H. C.; Shih, Y. C.; Chou, S. H.; Tseng, H. W.; Liu, C. P.; Tu, C. M.; Hu, T. L.; Tsai, Y. J.; Chern, J. W. *Bioorg. Med. Chem. Lett.* **2010**, *18*, 4674.
24. Tripathy, R.; Reiboldt, A.; Messina, P. A.; Iqbal, M.; Singh, J.; Bacon, E. R.; Angeles, T. S.; Yang, S. X.; Albom, M. S.; Robinson, C.; Chang, H.; Ruggeri, B. A.; Mallamo, J. P. *Bioorg. Med. Chem. Lett.* **2006**, *16*, 2158.
25. Tripathy, R.; Ghose, A.; Singh, J.; Bacon, E. R.; Angeles, T. S.; Yang, S. X.; Albom, M. S.; Aimone, L. D.; Herman, J. L.; Mallamo, J. P. *Bioorg. Med. Chem. Lett.* **2007**, *17*, 1793.
26. Han, S. Y.; Choi, J. W.; Yang, J.; Chae, C. H.; Lee, J.; Jung, H.; Lee, K. H.; Ha, J. D.; Kim, H. R.; Cho, S. Y. *Bioorg. Med. Chem. Lett.* **2012**, *22*, 2837.
27. Prakash, C. R.; Theivendren, P.; Raja, S. *Pharmacol. Pharm.* **2012**, *3*, 62. and references within for Sutent, SU5416, and SU6668.
28. Basal levels of KDR phosphorylation are relatively low in mouse lung tissue. Consequently, VEGF was administered i.v. 30 min prior to termination of the experiment to stimulate phosphorylation of KDR.
29. Khristich, B. I.; Simonov, A. M.; Shepelenko, E. N.; Yatsimirskii, V. A. *Chem. Heterocycl. Compd.* **1983**, *19*, 87.
30. Sun, L.; Tran, N.; Tang, F.; App, H.; Hirth, P.; McMahon, G.; Tang, C. *J. Med. Chem.* **1998**, *41*, 2588.
31. Detailed experimentals for this manuscript are found in the following patent: Bannen, L. C.; Brown, S. D.; Cheng, W.; Co, E.W.; Nuss, J. M.; Kim, M. H.; Klein, R. R.; Le, D. T.; Lew, A.; Mac, M. B.; Parks, J. J.; Wen, Z.; Xu, W. WO 2004050681 A2 **2004**.
32. Tang, P. C.; Sun, L.; McMahon, G.; Shawver, L. K.; Hirth, K. P. WO 9850356 A1 **1998**.
33. Guan, H.; Laird, A. D.; Blake, R. A.; Tang, C.; Liang, C. *Bioorg. Med. Chem. Lett.* **2004**, *14*, 187.
34. Walsh, D. A.; Moran, H. W.; Shamblee, D. A.; Uwaydah, I. M.; Welstead, W. J.; Sancilio, L. F.; Dannenburg, W. N. *J. Med. Chem.* **1984**, *27*, 1379.
35. *Kinase Inhibition Assays* Kinase activities of KDR and PDGFRa were measured as the percent of ATP consumed following the kinase reaction using luciferase-luciferin-coupled chemiluminescence as described previously.[36] Briefly, kinase reactions were initiated by combining test compound, ATP, kinases and substrates in a 20 mL volume using 384-well microtiter plates. For KDR, the final reaction mixture contained 3 mM ATP, 1.6 mM poly(Glu, Tyr) 4:1 (Sigma, St. Louis, MO) and 1.5 nM KDR of residues D807-V1356 with an N-terminal GST tag (ProQinase, Germany). For PDGFRa, the final reaction mixture contained 2 mM ATP, 10 mM MBP (Sigma) and 14 nM PDGFRa of residues Q551-L1089 with an N-terminal GST tag (ProQinase). The reaction mixture was incubated at room temperature for 4 h (KDR) or 2 h (PDGFRa) before a 20 mL aliquot of Kinase Glo (Promega, Madison, WI) was added and luminescence signal was measured using a Victor[2] plate reader (Perkin Elmer). Total ATP consumption was limited below 50%.
Activities of Flt1 and FGFR1 were measured using AlphaScreen as described previously.[37] Briefly, 0.13 nM N-terminal GST-tagged cytoplasmic Flt1 (ProQinase), or 0.09 nM N-terminal GST-tagged cytoplasmic FGFR1 was incubated with 3 nM biotinylated poly(Glu,Tyr) peptide, 5 or 3 μM ATP for 60 or 30 min, respectively.
36. Gendreau, S. B.; Venture, R.; Keast, P.; Laird, A. D.; Yakes, F. M.; Zhang, W.; Bentzien, F.; Cancilla, B.; Lutman, J.; Chu, F.; Jackman, L.; Shi, Y.; Yu, P.; Wang, J.; Aftab, D. T.; Jaeger, C. T.; Meyer, S. M.; De Costa, A.; Engell, K.; Chen, J.; Martini, J.; Joly, A. H. *Clin. Cancer Res.* **2007**, *13*, 3713.
37. Qian, F. E. S.; Yamaguchi, K.; Yu, P.; Won, K.; Mock, L.; Lou, T.; Tan, J.; Li, C.; Tam, D.; Lougheed, J.; Yakes, F. M.; Bentzien, F.; Xu, W.; Zaks, T.; Wooster, R.; Greshock, J.; Joly, A. H. *Cancer Res.* **2009**, *69*, 8009.
38. *FGF-stimulated ERK phosphorylation ELISA*: SK-N-MC (ATCC) cells were seeded at 4×10^4cells/well onto 96-well microtiter plates (Costar 3904), in MEME (Cellgro) containing 10% FBS (heat-inactivated, hyclone) and 1% penicillin–streptomycin (Cellgro). The cells were then incubated for 48 h at 37 °C in a humidified, 5% CO_2 atmosphere. DMSO or serial dilutions of test compounds in fresh serum-free medium were added to the cells and incubated for 1 h prior to recombinant human fibroblast growth factor basic FGF_{157} stimulation (25 ng/ml, R&D Systems, 234-FSE-025/CF) for 30 min. Negative control wells were not treated with growth factor. After treatment, medium was removed and cells were fixed followed by quenching of endogenous peroxidases with 0.6% H_2O_2 (Sigma). Fixed cells were then incubated in PBS containing 0.1% Triton X-100 and 10% FBS (heat-inactivated, Hyclone) for 1 h followed by incubation with anti-phosphorylated p44/42 MAPK, E10 (1:2,000, Cell Signaling, 9106) diluted in PBS containing 0.1% Triton X-100 and 1% BSA. Cells were then incubated for 1 h in PBS containing 0.1% Triton X-100 and 1% BSA with HRP-conjugated, goat anti-mouse (1:3,000, Jackson ImmunoResearch) antibody. A luminol-based substrate solution (Pierce, 37075) was added and measurements were taken in a Victor Wallac V plate reader (Perkin Elmer). The percentage inhibition of FGF_{157}-mediated Erk phosphorylation was calculated based on the ratio of the phosphorylated Erk luminescence measurement for compound-treated and FGF_{157}-stimulated samples to the phosphorylated Erk luminescence measurement for the DMSO-treated and FGF_{157}-stimulated samples. Percentage inhibition values at eight different compound concentrations were used to calculate IC_{50} values.
39. *VEGF-stimulated ERK phosphorylation ELISA*: Primary human umbilical vein endothelial cells (HUVEC, ATCC) were seeded at 2×10^4cells/well onto 96-well microtiter plates (Costar 3904), in EBM-2 (Clonetics) containing supplements (EGM-2 BulletKit, Clonetics). The cells were then incubated for 24 h at 37 °C in a humidified, 5% CO_2 atmosphere. Growth medium was replaced with serum-free EBM-2 and cells were incubated for an additional 24 h. DMSO or serial dilutions of test compounds in fresh serum-free medium were added to the cells and incubated for 1 h prior to recombinant human vascular endothelial growth factor $VEGF_{165}$ stimulation (20 ng/mL, R&D Systems, 293-VE-010) for 5 minutes. Negative control wells were not treated with growth factor. After treatment, medium was removed and cells were fixed followed by quenching of endogenous peroxidases with 0.6% H_2O_2 (Sigma). Fixed cells were then incubated in PBS containing 0.1% Triton X-100 and 10% FBS (heat-inactivated, Hyclone) for 1 h followed by incubation with anti-phosphorylated p44/42 MAPK, E10 (1:2,000, Cell Signaling, 9106) diluted in PBS containing 0.1% Triton X-100 and 1% BSA. Cells were then incubated for 1 h in PBS containing 0.1% Triton X-100 and 1% BSA with HRP-conjugated, goat anti-mouse (1:3000, Jackson immuno research) antibody. A luminol-based substrate solution (Pierce, 37075) was added and measurements were taken in a Victor Wallac V plate reader (Perkin Elmer). The percentage inhibition of $VEGF_{165}$-mediated Erk phosphorylation was calculated based on the ratio of the phosphorylated Erk luminescence measurement for compound-treated and $VEGF_{165}$-stimulated samples to the phosphorylated Erk luminescence measurement for the DMSO-treated and $VEGF_{165}$-stimulated samples. Percentage inhibition values at eight different compound concentrations were used to calculate IC_{50} values.
40. *Solid tumor efficacy studies*: Female nu/nu mice (Taconic, Hudson, NY) were housed according to the Exelixis Institutional Animal Care and Use Committee guidelines. On day 0, cells were inoculated intradermally into the hind flank (2×10^6 cells, HT29) or subcutaneously into a noncleared mammary fat pad (1×10^6 cells, MBA-MB-231). When tumors reached ~100 mg (12-14 days after implantation), mice were randomized ($n = 10$/group) and treated orally once daily for 14 or 28 days with test article or saline vehicle. Body weights were collected daily, and tumor weights were collected twice weekly. Percent tumor growth inhibition values were expressed as follows: (1-[(mean treated tumor weight on the final day − mean tumor weight on day 0)/(mean vehicle tumor weight on the final day − mean tumor weight on day 0)] × 100). Statistical analysis of **8h**-treated tumors versus vehicle-treated tumors was done by one-way analysis of variance (ANOVA) with significance defined as $P < 0.05$.
41. Spectral data for (*Z*)-3-((4-chlorophenyl)(1*H*-imidazol-2-yl)methylene)-5-(1-ethylpiperidin-4-ylamino)indolin-2-one (**8h**).
^{1}H NMR (400 MHz, d_6-DMSO): δ 10.92 (s, 1H), 7.57 (d, 2H), 7.54 (s, 1H), 7.30 (d, 2H), 7.16 (s, 1H), 6.59 (d, 1H), 6.43 (d, 1H), 4.92 (s, 1H), 4.87 (d, 1H), 2.75 (d, 2H), 2.34 (q, 2H), 2.29 (m, 1H), 1.94 (t, 2H), 1.56 (d, 2H), 1.11 (m, 2H), 1.00 (t, 3H); Analytical HPLC, retention time = 6.69 min, 99% purity (conditions: YMC C18 150 × 4.6 column, gradient 5–95% MeCN/H_2O, in the presence of 0.1% TFA, 25 min run at 1.5 mL/min flow rate, λ = 254 nM); MS(EI) for $C_{25}H_{26}ClN_5O$: 448.2 (MH^+); Elemental analysis, Calcd for $C_{25}H_{26}ClN_5O$: C, 60.89; H, 6.35; N, 14.37; Cl, 7.13. Found: C, 61.08, H, 5.86, N, 13.96, Cl, 7.73.